Journal of Solid State Chemistry **162,** 195–203 (2001)
doi:10.1006/jssc.2001.9236, available online at http://www.idealibrary.com on IDEAL®

$Na_3Cr_2P_3S_{12}$ and $K_3Cr_2P_3S_{12}$: Two New One-Dimensional Thiophosphate Compounds with a Novel Structure

S. Coste, E. Kopnin, M. Evain, S. Jobic,[1] C. Payen, and R. Brec

Laboratoire de Chimie des Solides, Institut des Matériaux Jean-Rouxel, UMR C6502 CNRS – Université de Nantes, 2 rue de la Houssinière, BP 32229, 44322 Nantes Cedex 3, France
E-mail: jobic@cnrs-imn.fr

Received December 18, 2000; in revised form May 2, 2001; accepted May 11, 2001

IN HONOR OF PROFESSOR PAUL HAGENMULLER ON THE OCCASION OF HIS 80TH BIRTHDAY

Two new alkali metal chromium thiophosphates, $Na_3Cr_2P_3S_{12}$ and $K_3Cr_2P_3S_{12}$, have been synthesized and their structure determined from single-crystal or powder X-ray diffraction analyses. These isostructural compounds, which exhibit a novel structural arrangement, crystallize in the monoclinic system (space group $P2_1/c$) with the cell parameters $a = 17.4076(10)$ Å, $b = 11.1723(10)$ Å, $c = 19.2502(11)$ Å, $\beta = 149.731(3)^\circ$ ($V = 1887.1(2)$ Å^3, $Z = 4$) and $a = 17.9690(14)$ Å, $b = 12.0607(5)$ Å, $c = 19.3109(16)$ Å, $\beta = 150.008(3)^\circ$ ($V = 2091.98(16)$ Å^3, $Z = 4$) for $Na_3Cr_2P_3S_{12}$ (I) and $K_3Cr_2P_3S_{12}$ (II), respectively. For (I), the single-crystal refinement led to $R/R_w(F^2) = 0.0417/0.0650$ (for 4125 independent reflections and 182 refined parameters). For (II), the Rietveld refinement led to $R_p/R_{wp} = 0.0181/0.0233$ (for 90 refined parameters). In both materials, the structures consist of $^1_\infty[Cr_2P_3S_{12}]^{3-}$ chains built upon two edge-sharing $[CrS_6]$ octahedra capped by two $[PS_4]$ tetrahedra defining isolated $[Cr_2P_2S_{12}]^{-8}$ entities. These entities are linked to each other through an extra $[PS_4]$ tetrahedral group. Magnetic measurements evidence antiferromagnetic coupling between Cr^{3+} cations. The charge balance of the phase is $M^I_3Cr^{III}_2P^V_3S^{-II}_{12}$. © 2001 Elsevier Science

Key Words: **one-dimensional compound; thiophosphate; chromium; X-ray diffraction; crystal structure; magnetism.**

1. INTRODUCTION

The reactive flux method using polychalcogenides A_xQ_y (A = alkali metal, Q = S, Se) has produced a wide variety of low-dimensional compounds (1–4). One of the interests of the method lies in its ability to control the covalent network dimensionality by modifying the nature of the alkali metal and its concentration to obtain a more or less covalent framework (5–7). This method has been recently successful in synthesizing new families of materials with the same elements but different stoichiometries (for instance $K_3Ce_2P_3S_{12}$ (3D), $K_2CeP_2S_7$ (2D), $KCeP_2Q_6$ (2D) (with Q = S, Se), $K_3CeP_2S_8$ (1D), and $K_9CeP_4S_{16}$ (0D) (8–10)). Following this procedure, the preparation of new thiophosphates of chromium and alkali metal were attempted through the exploration of the A/Cr/P/S system (A = Na or K). Compounds were found with either $^2_\infty[CrP_2S_7]^-$ layers as in $KCrP_2S_7$ (11) or $^1_\infty[CrP_2S_6]^-$ and $^1_\infty[CrP_2S_7]^{2-}$ chains as in $NaCrP_2S_6$ (12) and in $K_2CrP_2S_7$ (13), respectively, or $[Cr_2P_4S_{16}]^{6-}$ isolated units as in $K_3CrP_2S_8$ (14). All these materials have their anionic network stabilized by strong covalent bonds and their overall structure assured by weaker ionic interactions between the anionic network and the alkali metal cations. A potentially interesting property of these low-dimensional compounds may be their exfoliation in polar solvent. Recently, several studies have been carried out on 1D compounds to examine their chemical and physical behavior in organic solvents. Let us mention for instance the $KNiPS_4$ and $KPdPS_4$ (15, 16) and $LiMo_3Se_3$ (17–19) studies. Hence, while $^1_\infty[NiPS_4]^-$ chains undergo an autofragmentation under the action of the solvent to give rise to unprecedented discrete crown-shape $[Ni_3P_3S_{12}]^{3-}$ anions, $^1_\infty[PdPS_4]^-$ and $^1_\infty[Mo_3Se_3]^-$ chains are maintained in solution, which leads to a complex fluid and a liquid crystal behavior, respectively. Before reporting similar studies for various phases in the A/Cr/P/S system, we describe in this article the synthesis, X-ray structure determination, and magnetic properties of two new 1D compounds: $Na_3Cr_2P_3S_{12}$ and $K_3Cr_2P_3S_{12}$.

2. EXPERIMENTAL

2.1. Synthesis

The starting materials used to synthesize $K_3Cr_2P_3S_{12}$ and $Na_3Cr_2P_3S_{12}$ were Na_2S_3 and K_2S_3 prepared in liquid ammonia (20) (obtained from a stoichiometric mixture of

[1]To whom correspondence should be addressed. Fax: (33) 2 40 37 39 95.

0022-4596/01 $35.00
© 2001 Elsevier Science
All rights reserved.

elemental sodium or potassium and sulfur), Cr ($\geq 99\%$, Buchs), P_2S_5 or P (Fluka), and S (99.999%, Fluka). All phases were handled in a dry box under nitrogen (O_2 and H_2O content < 5 ppm).

2.1.1. $Na_3Cr_2P_3S_{12}$. Amounts of 0.3278 g (2.3 mmol) of Na_2S_3, 0.5124 g (2.3 mmol) of P_2S_5, and 0.1598 g (3.1 mmol) of Cr were thoroughly mixed and subsequently sealed under vacuum ($< 10^{-2}$ Pa) in a silica tube. The reaction mixture was heated up to 650°C at a rate of 6°C/h. The temperature was kept at 650°C for 1 week and then cooled down to room temperature at the rate of 5°C/h. The resulting sample, which turned out to be always polyphasic, contained both air-sensitive dark green needle-like crystals of $Na_3Cr_2P_3S_{12}$ and dark red plate-like crystals of $CrPS_4$. An EDXS (energy dispersive X-ray spectroscopy) analysis by means of a Jeol microscope (PGT-IMIX-PTS equiped Jeol-JSM5800LV) indicated the compositions $Na_{3.1}Cr_{2.0}P_{2.9}S_{12.2}$ for $Na_3Cr_2P_3S_{12}$ and $Cr_{1.1}P_{1.0}S_{4.3}$ for $CrPS_4$.

2.1.2. $K_3Cr_2P_3S_{12}$. Amounts of 0.3742 g (2.1 mmol) of K_2S_3, 0.1488 g (2.9 mmol) of Cr, 0.1329 g (4.3 mmol) of P, and 0.3670 g (11.4 mmol) of S were thoroughly mixed and subsequently sealed under vacuum ($< 10^{-2}$ Pa) in a silica tube. The reaction mixture was heated up to 600°C at the rate of 6°C/h. The temperature was kept at 600°C for 1 week and then cooled down to room temperature at the rate of 5°C/h. The sample was pure and contained only air-sensitive dark green needle-like crystals. EDXS analyses of several crystals yielded the phase composition: $K_{3.2}Cr_2P_{2.9}S_{12.3}$ for $K_3Cr_2P_3S_{12}$.

2.2. Structure Determination of $Na_3Cr_2P_3S_{12}$

2.2.1. Data collection. Needle-like crystals of $Na_3Cr_2P_3S_{12}$ were isolated from the as-prepared sample, glued in Lindemann quartz capillaries by means of epoxy resin, and tested on a STOE imaging plate diffraction system. They immediately appeared as systematically twinned (multiple twinning). A crystal, with apparently only two twin domains (one strong and one weak), was selected. Reflection intensities were then collected at room temperature on the STOE diffractometer, in a medium resolution setup (IP at 60 mm, limiting $\sin(\theta)/\lambda$ values to 0.65 Å^{-1}). Intensity integration was carried out for the main domain, regardless of the possible overlapping of the reflections, although both domain orientation matrices could be obtained. The refinement of the cell parameters, obtained from 6042 reflections, led to $a = 17.4076(10)$ Å, $b = 11.1723(10)$ Å $c = 19.2502(11)$ Å, $\beta = 149.731(3)°$, and $V = 1887.1(2)$ Å^3.

2.2.2. Structure refinement. The 21,309 intensities of the collected reflection set were corrected for Lorentz polarization with the STOE IPDS software package (21). The structure was easily solved by means of the SHELXS direct methods (22), regardless of the twinning. Subsequent calculations were carried out with the JANA2000 package crystallographic program (23). After the absorption correction (analytical, Gaussian-type integration), the redundant set of reflections was merged according to the $2/m$ point group. Taking into account the twinning, this yielded $R_{int}(\text{obs}) = 0.0771$ (4125 independent reflections, of which 2045 were observed at a $2\sigma(I)$ level). Introducing atoms with initially isotropic and then anisotropic displacement parameters the F^2 residue factor quickly converged to $R = 0.0498$ for 182 parameters. Removing partially overlapping reflections (Jana2000 CHECKRAN option), the residual factor dropped to 0.0417 for 3638 reflections (at a $2\sigma(I)$ level).

2.3. Structure Determination of $K_3Cr_2P_3S_{12}$

2.3.1. Data collection. As suitable crystals could not be found for single structural determination, the $K_3Cr_2P_3S_{12}$ structure was refined from an X-ray diffraction powder pattern. Only the approximate cell parameters and the space group were determined on a heavily twinned crystal. These data showed $K_3Cr_2P_3S_{12}$ to be isostructural with the sodium derivative. A powder without detectable impurities was sieved at 50 μm and introduced, under a dry argon atmosphere, in a Lindemann capillary (0.1 mm in diameter). The powder pattern was recorded at room temperature on an INEL diffractometer using a monochromatized radiation CuK–L_2 ($\lambda = 1.54059$ Å), equipped with a CPS 120 detector in a Debby–Sherrer geometry setup.

2.3.2. Structure refinement. The $K_3Cr_2P_3S_{12}$ structure refinement was carried out with Jana2000 (23). In a first step, a Le Bail analysis (24) of the diagram ($8 < 2\theta < 104°$, $\Delta 2\theta$ step $= 0.03$, number of reflections $= 2338$) led to accurate cell parameters, peak shape (pseudo-Voigt), and approximate background (Chebyschev polynoms). Then a Rietveld refinement (25) of the structure was carried out, starting from the $Na_3Cr_2P_3S_{12}$ structural model ($P2_1/c$ space group, $Z = 4$). Given the weak intensity of the powder pattern at high 2θ values, K, Cr, and P isotropic displacement parameters were constrained to be the same for each atomic species. In addition, the P–S distances were restrained to vary in the range 1.87–2.17 Å according to the interatomic distances reported in the literature (26). In the final stage, the residual factors converged to $R_p = 0.0181$ and $R_{WP} = 0.0233$. The refined cell parameters are $a = 17.9690(14)$ Å, $b = 12.0607(5)$ Å, $c = 19.3109(16)$ Å, $\beta = 150.008(3)°$, $V = 2091.98(16)$ Å^3. The final X-ray powder pattern with the Rietveld profile and difference diagram is reported in Fig. 1.

Data collection parameters and refinement conditions and results for $Na_3Cr_2P_3S_{12}$ and $K_3Cr_2P_3S_{12}$ are summarized in the Tables 1a and 1b, respectively. Atomic coordinates and displacement parameters are given in Tables 2a

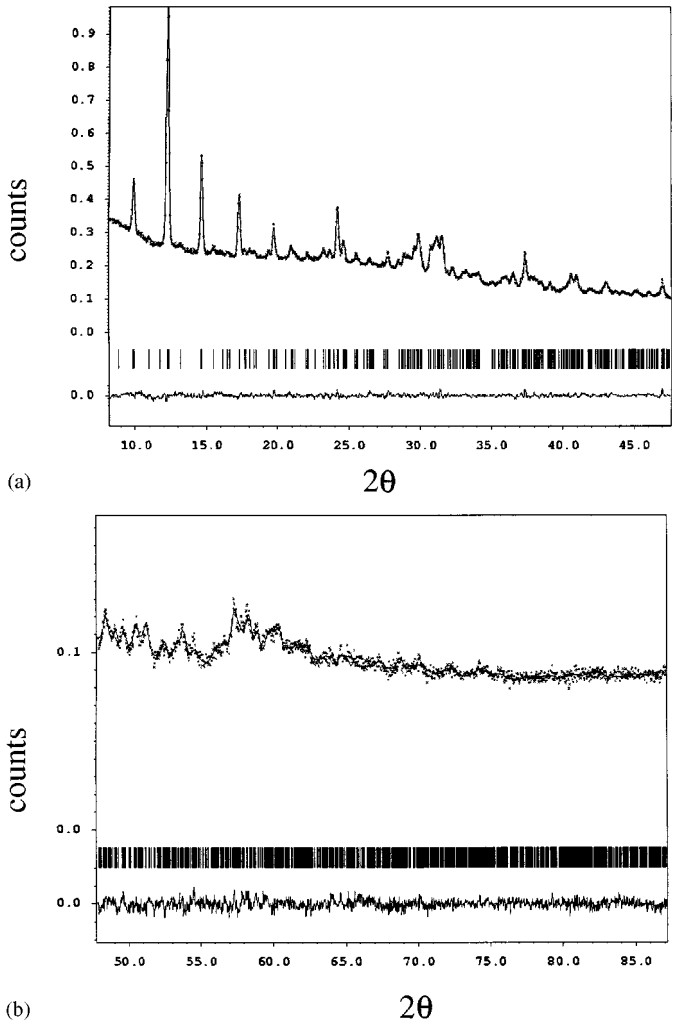

FIG. 1. Observed (doted line), calculated (solid line), and difference X-ray powder patterns obtained from the Rietveld refinement of $K_3Cr_2P_3S_{12}$.

and 2b. Anisotropic displacement parameters of $Na_3Cr_2P_3S_{12}$ are given in Table 3.

3. STRUCTURE DESCRIPTION

The $Na_3Cr_2P_3S_{12}$ and $K_3Cr_2P_3S_{12}$ isostructural compounds consist of $^1_\infty[Cr_2P_3S_{12}]^{3-}$ one-dimensional chains separated by the alkali metal cations (Fig. 2). Each chain is built upon $[Cr_2S_{10}]^{14-}$ units obtained from two edge-sharing $[CrS_6]$ octahedra. Each $[Cr_2S_{10}]^{14-}$ bioctahedron is capped, above and below, by two extra $[PS_4]^{3-}$ tetrahedral units sharing two apical and one bidentated equatorial sulfur to form $[Cr_2P_2S_{12}]^{8-}$ dimers. These dimers are then linked to each other by $[PS_4]^{3-}$ tetrahedral groups through edge sharing (Fig. 2) to form the $^1_\infty[Cr_2P_3S_{12}]^{3-}$ isolated chains. Note that these chains contain $[Cr_2P_4S_{16}]^{6-}$ blocks similar to those already observed in 0D-$K_3CrP_2S_8$ (14). These chains may also be considered as deriving

TABLE 1a
Crystal, X-Ray Data Collection, and Refinement Parameters for $Na_3Cr_2P_3S_{12}$

1. Physical, crystallographic, and analytical data	
Chemical formula	$Na_3Cr_2P_3S_{12}$
Molecular weight (g.mol^{-1})	650.6
Density	2.289
Crystal system	Monoclinic
Space group	$P2_1/c$
Cell parameters	
a (Å)	17.4076(10)
b (Å)	11.1723(10)
c (Å)	19.2502(11)
β (°)	149.731(3)
V (Å^3)	1887.1(2)
Z	4
No. of reflections for cell parameters	6042
Crystal description	Needle
Color	Dark green
Crystal size (mm^3)	$0.31 \times 0.08 \times 0.03$
2. Data collection	
Temperature (K)	293
Diffractometer	Stoe IPDS
Radiation	MoK–$L_{2,3}$ (0.71073 Å)
Monochromator	Oriented graphite (002)
Scan mode	ω
$\sin(\theta)/\lambda$ range (Å^{-1})	0–0.65
hkl range	$-22 \le h \le 22$ $-14 \le k \le 14$ $-22 \le l \le 22$
Number of reflections	21309
3. Data reduction	
Absorption correction	Analytical
T_{min}/T_{max}	0.6144–0.6973
No. of independent reflections	4125
Criterion for observed reflections	$I > 2\sigma(I)$
R_{int} (obs)	0.0771
No. of observed reflections	2045
4. Refinement results[a]	
Refinement	F^2
$F(000)$	1272
Reflections used in the refinement (all)	3638
Reflections used in the refinement (obs)	1800
Refined parameters	182
$(\Delta/\sigma)_{max}$	< 0.001
Twin matrix (defined with respect to the row indices)	$\begin{pmatrix} 1 & 0 & 0 \\ 0 & -1 & 0 \\ 1.5636 & 0 & -1 \end{pmatrix}$
Twin fractions (%)	9.3(2)
R (obs)[a]	0.0417
R_w (obs)[a]	0.0650
R (all)[a]	0.1206
R_w (all)[a]	0.0892
Weighting scheme	$w_{F^2} = 1/(\sigma^2(I_0) + (2 \times 0.016 \times I_0)^2)$
Difference Fourier residues (e$^-$/Å$_3$)	[1.68, −1.61]

[a] $R = \sum||F_o| - |F_c||/\sum|F_o|$. $wR_{F^2} = [\sum w_{F^2}(|F_o|^2 - |F_c|^2)^2/\sum w_{F^2}|F_o|^4]^{1/2}$.

TABLE 1b
Crystal, X-ray Data Collection, and Refinement Parameters for $K_3Cr_2P_3S_{12}$

Chemical formula	$K_3Cr_2P_3S_{12}$
Molecular weight (g.mol^{-1})	698.98
Crystal system	Monoclinic
Space group	$P2_1/c$
Crystal description	Needle
Color	Dark green
Cell parameters	
a	17.9690(14) Å
b	12.0607(5) Å
c	19.3109(16) Å
β	150.008(3)°
V	2091.98(16) Å^3
Halfwidth parameters	
GU	0.119(11)
GV	−0.042(4)
GW	0.00083 (4)
LY	0.0034(2)
Asymetry parameters ($2\theta < 40°$)[a]	
S/L	0.011377
H/L	0.012731
Preferred orientation[b]	0.962(6)
Reliability factors[c]	$R_p = 0.0181$ $R_{wp} = 0.0233$ $\chi^2 = 1.62$
Refined parameters	90

Note. More realisitic e.s.d.'s can be achieved by applying the Berar's factor: 1.793 (31).

[a] Reference (32).

[b] References (33) and (34).

[c] $R_p = \sum|I_0 - I_C|/\sum I_0$, $R_{WP} = \sqrt{\sum w(I_0 - I_C)^2/\sum wI_0^2}$.

TABLE 2a
Fractional Atomic Coordinates, Equivalent Isotropic Displacement Parameters (Å^2) and s.u.'s for $Na_3Cr_2P_3S_{12}$

Atom	X	Y	Z	U_{eq}[a]
Na(1)	0.2005(6)	0.1271(4)	−0.0033(4)	0.070(8)
Na(2)	1.2894(6)	0.0850(4)	0.7387(6)	0.063(10)
Na(3)	1.3120(7)	0.4168(4)	0.9567(6)	0.093(13)
Cr(1)	0.79612(14)	0.28039(12)	0.39642(13)	0.014(2)
Cr(2)	0.78330(14)	0.26813(11)	0.57204(13)	0.013(2)
P(1)	0.7799(2)	0.2617(2)	0.2265(2)	0.015(2)
P(2)	1.0578(2)	0.18244(19)	0.6946(2)	0.015(3)
P(3)	0.5258(2)	0.3685(2)	0.2769(2)	0.018(3)
S(1)	0.9560(2)	0.35291(18)	0.6184(2)	0.017(3)
S(2)	0.6253(2)	0.19745(17)	0.3520(2)	0.015(3)
S(3)	0.9590(2)	0.10402(19)	0.7024(2)	0.021(3)
S(4)	0.6107(2)	0.4382(2)	0.4332(2)	0.022(3)
S(5)	0.9722(2)	0.1157(2)	0.5377(2)	0.022(3)
S(6)	0.6248(2)	0.4505(2)	0.2703(2)	0.025(3)
S(7)	0.6519(2)	0.1753(2)	0.1990(2)	0.020(3)
S(8)	0.9075(2)	0.1482(2)	0.2679(2)	0.020(3)
S(9)	0.6391(2)	0.3415(2)	0.0450(2)	0.022(3)
S(10)	1.2826(2)	0.1872(2)	0.8738(2)	0.033(3)
S(11)	0.9090(2)	0.3776(2)	0.3843(2)	0.025(3)
S(12)	0.2993(2)	0.3656(2)	0.0969(2)	0.033(3)

[a] $U_{eq} = \frac{1}{3}\sum_i\sum_j U^{ij}a_i^*a_j^*\mathrm{a}_i\mathrm{a}_j$.

from the $^1_\infty[CrP_2S_7]^{2-}$ chains observed in 1D-$K_2CrP_2S_7$ (13) in which one $[P_2S_6]$ ethane-like group linking two $[Cr_2P_2S_{12}]$ building block is replaced by a $[PS_4]$ tetrahedron.

The $[Cr_2P_3S_{12}]^{3-}$ chains of $Na_3Cr_2P_3S_{12}$ and $K_3Cr_2P_3S_{12}$, running along the c axis are contained in planes parallel to [010] with their capping protuberances alternating to optimize the packing (Fig. 2). The chains are separated by the Na^+ or K^+ alkali metal cations, which approximately occupy the midpoint between three neighboring $[Cr_2P_3S_{12}]^{3-}$ chain axes (Fig. 3).

In Tables 4a and 4b are gathered the main P–S and Cr–S interatomic distances and the S–P–S and S–Cr–S angles observed in $Na_3Cr_2P_3S_{12}$ and $K_3Cr_2P_3S_{12}$. Let consider first $Na_3Cr_2P_3S_{12}$. The Cr–S distances and the cis S–Cr–S angles range from 2.376(4) to 2.473(4) Å ($\overline{Cr(1)–S} = 2.427$ Å and $\overline{Cr(2)–S} = 2.423$ Å), and from 81.99(15)° to 102.89(14)° ($\overline{S–Cr(1)–S} = 90.16°$ and $\overline{S–Cr(2)–S} = 90.10°$), respectively. Dispersion of the distances and the angles evidence a distortion of the $[CrS_6]$ octahedra. Nevertheless, the Cr–S distances agree well with the sum of the ionic radii $r(Cr^{3+}) + r(S^{2-}) = 2.45$ Å (26). Moreover, the Cr(1)–Cr(2) distances in the $[Cr_2S_{10}]$ bioctahedral entity is equal to 3.578(4) Å, and the Cr(1)–S(1)–Cr(2) and Cr(1)–S(2)–Cr(2) angles are calculated at 92.75(10)° and 93.59(10)°. These data agree well with those observed in $K_3CrP_2S_8$ (14)

TABLE 2b
Fractional Atomic Coordinates, Isotropic Displacement Parameters (Å^2), and s.u.'s for $K_3Cr_2P_3S_{12}$

Atoms	X	Y	Z	U_{iso}[a]
K(1)	0.800(2)	0.8716(19)	1.003(2)	0.060(5)
K(2)	0.721(2)	0.9159(16)	1.272(2)	0.060(5)
K(3)	0.710(2)	0.6001(18)	1.096(2)	0.060(5)
Cr(1)	0.2227(18)	0.7207(14)	0.6181(18)	0.057(4)
Cr(2)	0.218(2)	0.7272(16)	0.437(2)	0.057(4)
P(1)	0.244(2)	0.7408(19)	0.782(3)	0.010(5)
P(2)	−0.027(2)	0.8382(16)	0.327(2)	0.010(5)
P(3)	0.487(2)	0.6349(18)	0.741(2)	0.010(5)
S(1)	0.064(2)	0.6675(19)	0.399(2)	0.032(2)
S(2)	0.395(3)	0.797(2)	0.662(2)	0.032(2)
S(3)	0.091(3)	0.893(2)	0.338(3)	0.032(2)
S(4)	0.411(2)	0.582(2)	0.579(2)	0.032(2)
S(5)	0.071(2)	0.872(2)	0.504(2)	0.032(2)
S(6)	0.381(3)	0.560(2)	0.741(2)	0.032(2)
S(7)	0.383(2)	0.821(2)	0.821(2)	0.032(2)
S(8)	0.103(3)	0.832(2)	0.727(2)	0.032(2)
S(9)	0.358(2)	0.684(2)	0.959(2)	0.032(2)
S(10)	−0.247(2)	0.8297(17)	0.140(2)	0.032(2)
S(11)	0.115(2)	0.609(2)	0.641(2)	0.032(2)
S(12)	0.714(2)	0.623(2)	0.936(2)	0.032(2)

[a] $U_{iso} = \frac{1}{3}\sum_i\sum_j U^{ij}a_i^*a_j^*\mathrm{a}_i\mathrm{a}_j$.

TABLE 3
Anisotropic Displacement Parameters $U^{ij a}$ (Å^2) and s.u.'s for $Na_3Cr_2P_3S_{12}$

Atom	U^{11}	U^{22}	U^{33}	U^{12}	U^{13}	U^{23}
Na(1)	0.072(2)	0.035(2)	0.041(2)	0.001(2)	0.040(2)	0.0013(19)
Na(2)	0.067(2)	0.063(3)	0.098(3)	0.014(2)	0.077(2)	0.017(2)
Na(3)	0.146(5)	0.043(2)	0.074(3)	−0.033(2)	0.093(3)	−0.016(2)
Cr(1)	0.0164(5)	0.0181(6)	0.0141(6)	0.0013(4)	0.0140(5)	0.0011(4)
Cr(2)	0.0162(5)	0.0155(6)	0.0141(6)	0.0012(4)	0.0139(5)	0.0003(4)
P(1)	0.0178(8)	0.0173(10)	0.0162(9)	0.0008(7)	0.0155(8)	0.0012(7)
P(2)	0.0131(8)	0.0182(9)	0.0131(9)	0.0029(7)	0.0112(8)	0.0022(7)
P(3)	0.0157(9)	0.0200(10)	0.0166(10)	0.0055(7)	0.0137(9)	0.0029(8)
S(1)	0.0211(8)	0.0146(9)	0.0196(9)	0.0000(7)	0.0184(8)	−0.0006(7)
S(2)	0.0187(8)	0.0158(8)	0.0171(9)	0.0016(7)	0.0163(8)	0.0011(7)
S(3)	0.0256(10)	0.0197(10)	0.0263(1)	0.0046(8)	0.0239(10)	0.0068(8)
S(4)	0.0235(9)	0.0253(10)	0.0202(10)	0.0062(8)	0.0194(9)	0.0016(8)
S(5)	0.0239(10)	0.0237(10)	0.0202(10)	0.0060(8)	0.0194(9)	0.0014(8)
S(6)	0.0323(11)	0.0224(10)	0.0307(12)	0.0099(8)	0.0288(10)	0.0104(8)
S(7)	0.0192(9)	0.0296(10)	0.0175(9)	−0.0061(7)	0.0167(8)	−0.0038(8)
S(8)	0.0211(9)	0.0239(10)	0.0190(10)	0.0073(8)	0.0178(9)	0.0062(8)
S(9)	0.0232(9)	0.0278(11)	0.0212(9)	0.0096(8)	0.0203(9)	0.0096(8)
S(10)	0.0144(9)	0.0382(12)	0.0205(11)	0.0031(8)	0.0113(9)	0.0029(9)
S(11)	0.0333(11)	0.0268(11)	0.0289(11)	−0.0115(8)	0.0288(10)	−0.0100(8)
S(12)	0.0185(9)	0.0352(12)	0.0201(11)	0.0057(9)	0.0132(9)	0.0010(9)

[a]The harmonic displacement factor exponent takes the form $-2\pi^2 \sum_i \sum_j U^{ij} a_i^* a_j^* h_i h_j$.

(Cr–Cr = 3.523(1) Å, $\overline{\text{S–Cr–S}} = 91.08°$). The $[PS_4]^{3-}$ tetrahedra are also distorted but this distortion is highly dependent on the $[PS_4]$ chemical environment. Hence, in the $[P(1)S_4]$ units (Fig. 2), the P–S distances and the cis S–P–S angles range only from 2.028(6) to 2.054(4) Å ($\overline{\text{P(1)–S}} = 2.039$ Å) and from 103.5(3)° to 114.77(16)° ($\overline{\text{S–P–S}} = 109.52°$) respectively. In contrast, the two capping $[P(2)S_4]$ and $[P(3)S_4]$ units of the $[Cr_2P_2S_{12}]$ blocks (Fig. 2) are, as expected, much more distorted. The P–μ_1S is shorter (1.974(2) for P(2)–S and 1.989(2) Å for P(3)–S) than the P–μ_2S distances (2.032(6) and 2.047(7) Å for P(2)–S and 2.039(6) and 2.051(7) Å for P(3)–S), which are themselves shorter than the P–μ_3S distances (2.105(3) for $\overline{\text{P(2)–S}}$ and 2.101(3) Å for P(3)–S) ($\overline{\text{P(2)–S}} = 2.039$ Å, $\overline{\text{P(3)–S}} = 2.045$ Å). Otherwise, the S–P–S cis angles range from 100.6(2)° to 114.2(3)° and from 102.2(2)° to 113.56(13)°

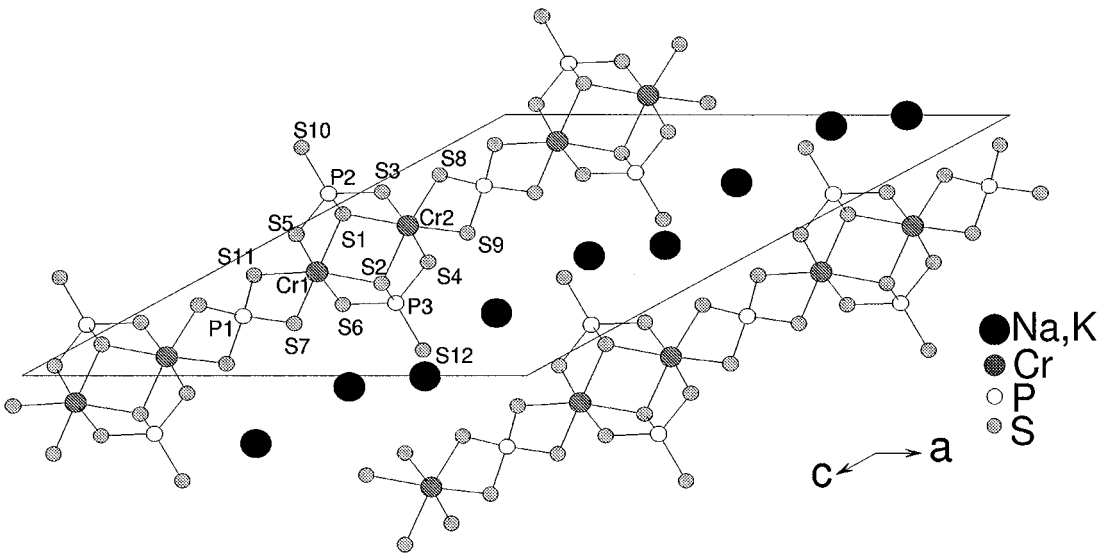

FIG. 2. View of the $Na_3Cr_2P_3S_{12}$ structure along the *b* axis. The chains are built from edge (S(1)–S(2)) sharing between $[Cr(1)S_6]$ and $[Cr(2)S_6]$ octaedra. The $[CrS_{10}]$ units are linked to each other by $[P(1)S_4]$ edge-sharing groups. Each $[Cr_2S_{10}]$ bioctahedron is capped by $[P(2)S_4]^{3-}$ and $[P(3)S_4]^{3-}$ tetrahedral units sharing two apical (S(5), S(3) and S(6), S(4) respectively) and one bidentated equatorial (S(1) and S(2)) sulfur atoms.

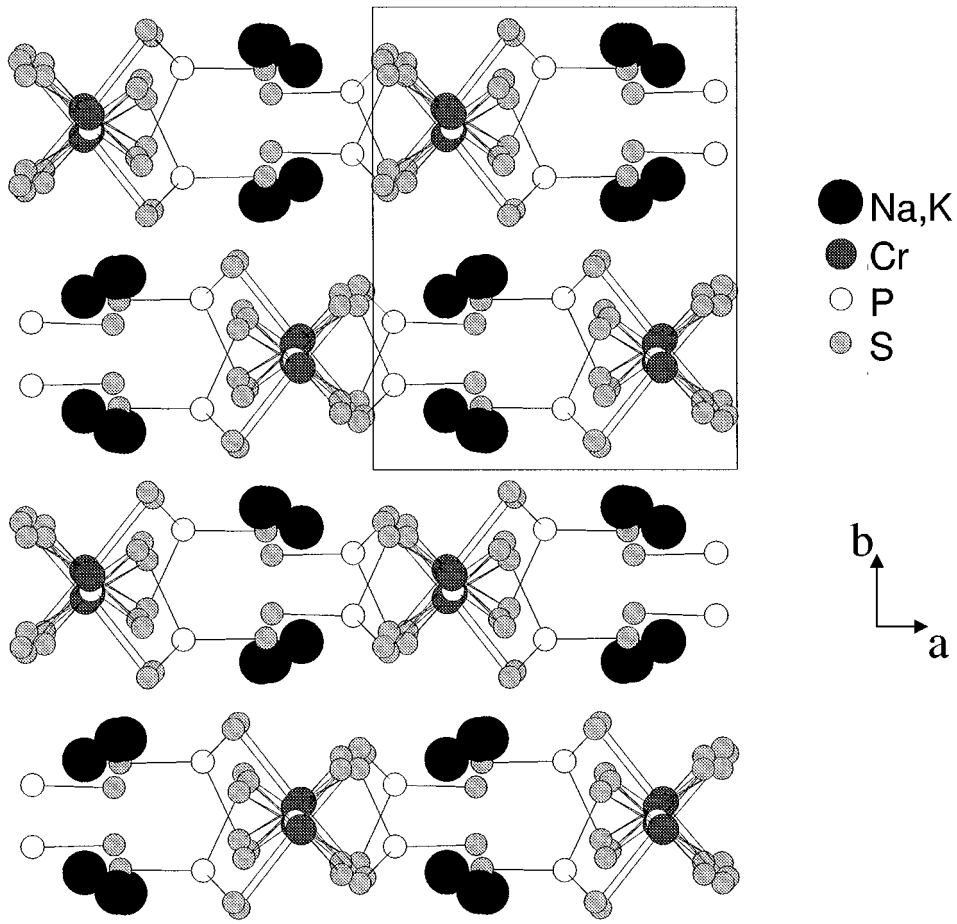

FIG. 3. View of the $Na_3Cr_2P_3S_{12}$ structure along the c axis showing the stacking of the infinite $^1_\infty[Cr_2P_3S_{12}]^{3-}$ chains.

for P(2) and P(3), respectively. These observations fit well with previous reported discussion on $[Ni_3P_3S_{12}]^{3-}$ (16). The three different sodium cations are coordinated by six sulfur atoms with Na–S distances ranging from approx. 2.83 to 3.49 Å. The average distances ($\overline{Na(1)–S}$ = 3.11 Å, $\overline{Na(2)–S}$ = 3.05 Å, and $\overline{Na(3)–S}$ = 3.07 Å) agree well with sodium–sulfur distances found for such a coordination of the alkali metal (26). Following all the above considerations, the charge balance must be written $Na^{I}_3Cr^{III}_2P^{IV}_3S^{-II}_{12}$.

Compared to $Na_3Cr_2P_3S_{12}$, the $[CrS_6]$ octahedra and $[PS_4]$ tetrahedra in $K_3Cr_2P_3S_{12}$ appear much more distorted (Table 4b). However, it should be noted that this may be only related to the accuracy on the atomic positions, which are rather low because of the poor quality of the powder pattern (important peak overlaps for $2\theta > \sim 45^\circ$). Despite higher standard uncertainties (s.u.), a good agreement of the experimental distances $\langle Cr–S \rangle$ = 2.42 Å, $\langle P–S \rangle$ = 2.09 Å, and $\langle K–S \rangle$ = 3.34 Å with the sum of the ionic radii (2.45, 2.01, and 3.22 Å, respectively) is observed.

4. MAGNETIC PROPERTIES OF $K_3Cr_2P_3S_{12}$

Magnetic measurements were carried out on a commercial SQUID magnetometer using powder samples. The magnetization M was measured as a function of field at both low and high (up to T = 300 K) temperatures to see if there was any evidence for ferromagnetic impurities. The magnetic susceptibility, $\chi = M/H$, was then determined in measuring fields H of 100 and 1000 Oe for temperatures between 2 and 300 K. Because of the persistent contamination of $Na_3Cr_2P_3S_{12}$ by $CrPS_4$, our magnetic data for $Na_3Cr_2P_3S_{12}$ could not be analyzed.

Figure 4 shows the temperature dependencies of the molar susceptibility and the reciprocal susceptibility for $K_3Cr_2P_3S_{12}$. These data were corrected for the diamagnetism of the constituent ions by using Pascal's constants ($\chi_{K(I)} = -13 \times 10^{-6}$, $\chi_{Cr(III)} = -11 \times 10^{-6}$, $\chi_{P(V)} = 1 \times 10^{-6}$, $\chi_{S(-II)} = -38 \times 10^{-6}$ emu/mol) (27). Above 100 K, the susceptibility obeys the Curie–Weiss law, $\chi = C/(T-\theta)$. The Curie constant C = 1.825(1) cm^3 K/Cr mol corresponds to an effective moment $\mu_{eff} = 3.82\,\mu_B$/Cr atom. These values

are consistent with Cr^{3+} in an octahedral environment having a spin $S = \frac{3}{2}$ (spin-only value: $\mu_{S.O.} = 3.87\ \mu_B$). The Weiss constant, $\theta = -11.1(2)$ K, indicates the presence of weak antiferromagnetic coupling between the chromium ions. Below 100 K, the susceptibility deviates from the Curie–Weiss behavior. The susceptibility curve exhibits a rounded maximum at 19 K and a weak peak at 7 K, which probably indicates the onset of a magnetic order.

Since the structure of $K_3Cr_2P_3S_{12}$ contains edge-sharing Cr_2S_{10} bioctahedra, the presence of magnetic coupling between the Cr^{III} ions within the bioctahedra was anticipated. As a basis for the interpretation of the data in the paramagnetic region (above 7 K), the simple isotropic Heisenberg Hamiltonian for two spin $S = \frac{3}{2}$ paramagnetic centers, $H = -2J\,S_1S_2$, was used, since the Cr^{III} ions have no orbital angular momentum associated with their $^3A_{1g}$ ground state. J is the (super)exchange coupling constant (negative for an antiferromagnetic interaction). The theoretical expression for the susceptibility $\chi(T)$ is obtained by using the Van Vleck equation, and the experimental data were fit using the following expression for a mole of dimers (28),

$$\chi(T) = \frac{2Ng^2\mu_B^2}{3kT}\left(\frac{42 + 15e^{3x} + 3e^{5x}}{7 + 5e^{3x} + 3e^{5x} + e^{6x}}\right), \qquad [1]$$

TABLE 4a
Main Interatomic Distances (Å), Angles (°), and Corresponding s.u.'s for $Na_3Cr_2P_3S_{12}$

$Cr(1)S_6$ group		$Cr(2)S_6$ group	
Cr(1)–S(1)	2.473(4)	Cr(2)–S(1)	2.469(5)
Cr(1)–S(2)	2.458(5)	Cr(2)–S(2)	2.450(4)
Cr(1)–S(5)	2.404(2)	Cr(2)–S(3)	2.399(2)
Cr(1)–S(6)	2.427(2)	Cr(2)–S(4)	2.430(2)
Cr(1)–S(7)	2.376(4)	Cr(2)–S(8)	2.384(4)
Cr(1)–S(11)	2.426(6)	Cr(2)–S(9)	2.410(5)
$\overline{Cr(1)–S}$	2.427	$\overline{Cr(2)–S}$	2.423
	Cr(1)–Cr(2) = 3.578(4)		
S(1)–Cr(1)–S(2)	86.69(17)	S(1)–Cr(2)–S(2)	86.97(17)
S(1)–Cr(1)–S(5)	82.16(12)	S(1)–Cr(2)–S(3)	81.99(15)
S(1)–Cr(1)–S(6)	92.80(14)	S(1)–Cr(2)–S(4)	93.45(15)
S(1)–Cr(1)–S(1)1	102.89(14)	S(1)–Cr(2)–S(8)	96.91(14)
S(2)–Cr(1)–S(5)	94.73(15)	S(2)–Cr(2)–S(3)	94.32(14)
S(2)–Cr(1)–S(6)	82.82(16)	S(2)–Cr(2)–S(4)	82.82(12)
S(2)–Cr(1)–S(7)	88.18(15)	S(2)–Cr(2)–S(9)	93.30(14)
S(5)–Cr(1)–S(7)	89.13(12)	S(3)–Cr(2)–S(8)	92.86(13)
S(5)–Cr(1)–S(1)1	95.99(11)	S(3)–Cr(2)–S(9)	89.24(15)
S(6)–Cr(1)–S(7)	95.66(11)	S(4)–Cr(2)–S(8)	90.24(14)
S(6)–Cr(1)–S(1)1	87.17(17)	S(4)–Cr(2)–S(9)	95.29(16)
S(7)–Cr(1)–S(1)1	83.79(18)	S(8)–Cr(2)–S(9)	83.90(18)
$\overline{S–Cr(1)–S}$	90.16	$\overline{S–Cr(2)–S}$	90.10
	Cr(1)–S(1)–Cr(2) = 92.75(10)		
	Cr(1)–S(2)–Cr(2) = 93.59(10)		

$P(1)S_4$ group		$P(2)S_4$ group		$P(3)S_4$ group	
P(1)–S(7)	2.034(7)	P(2)–S(1)	2.105(3)	P(3)–S(2)	2.101(3)
P(1)–S(8)	2.028(6)	P(2)–S(3)	2.047(7)	P(3)–S(4)	2.039(6)
P(1)–S(11)	2.041(4)	P(2)–S(5)	2.032(6)	P(3)–S(6)	2.051(7)
P(1)–S(9)	2.054(4)	P(2)–S(10)	1.974(2)	P(3)–S(12)	1.989(2)
$\overline{P(1)–S}$	2.039	$\overline{P(2)–S}$	2.039	$\overline{P(3)–S}$	2.045
S(7)–P(1)–S(8)	112.78(18)	S(1)–P(2)–S(3)	100.6(2)	S(2)–P(3)–S(4)	102.46(19)
S(7)–P(1)–S(9)	109.50(17)	S(1)–P(2)–S(5)	101.59(19)	S(2)–P(3)–S(6)	102.2(2)
S(7)–P(1)–S(11)	103.8(3)	S(1)–P(2)–S(10)	113.49(13)	S(2)–P(3)–S(12)	113.56(13)
S(8)–P(1)–S(9)	103.5(3)	S(3)–P(2)–S(5)	100.58(17)	S(4)–P(3)–S(6)	110.11(18)
S(8)–P(1)–S(11)	112.80(17)	S(3)–P(2)–S(10)	114.0(2)	S(4)–P(3)–S(12)	113.4(3)
S(9)–P(1)–S(11)	114.77(16)	S(5)–P(2)–S(10)	114.2(3)	S(6)–P(3)–S(12)	114.0(2)
$\overline{S–P(1)–S}$	109.52	$\overline{S–P(2)–S}$	107.41	$\overline{S–P(3)–S}$	109.29

TABLE 4b
Main Interatomic Distances (Å), Angles (°), and Corresponding s.u.'s for $K_3Cr_2P_3S_{12}$

$Cr(1)S_6$ group			$Cr(2)S_6$ group		
Cr(1)–S(1)	2.35(5)		Cr(2)–S(1)	2.29(7)	
Cr(1)–S(2)	2.56(7)		Cr(2)–S(2)	2.41(5)	
Cr(1)–S(5)	2.29(3)		Cr(2)–S(3)	2.30(3)	
Cr(1)–S(6)	2.40(3)		Cr(2)–S(4)	2.47(3)	
Cr(1)–S(7)	2.35(4)		Cr(2)–S(8)	2.59(7)	
Cr(1)–S(11)	2.68(6)		Cr(2)–S(9)	2.42(7)	
$\overline{Cr(1)–S}$	2.43		$\overline{Cr(2)–S}$	2.41	
		Cr(1)–Cr(2) = 3.43(7)			
S(1)–Cr(1)–S(2)	86(2)		S(1)–Cr(2)–S(2)	91(2)	
S(1)–Cr(1)–S(5)	84.7(13)		S(1)–Cr(2)–S(3)	87(2)	
S(1)–Cr(1)–S(6)	96.2(16)		S(1)–Cr(2)–S(4)	105.8(18)	
S(1)–Cr(1)–S(11)	103.3(15)		S(1)–Cr(2)–S(8)	108.4(16)	
S(2)–Cr(1)–S(5)	96.8(18)		S(2)–Cr(2)–S(3)	90.0(16)	
S(2)–Cr(1)–S(6)	84.6(19)		S(2)–Cr(2)–S(4)	81.5(13)	
S(2)–Cr(1)–S(7)	82.6(18)		S(2)–Cr(2)–S(9)	89.1(19)	
S(5)–Cr(1)–S(7)	85.0(13)		S(3)–Cr(2)–S(8)	94.1(19)	
S(5)–Cr(1)–S(11)	98(2)		S(3)–Cr(2)–S(9)	84(2)	
S(6)–Cr(1)–S(7)	94.4(11)		S(4)–Cr(2)–S(8)	90(2)	
S(6)–Cr(1)–S(11)	80.9(18)		S(4)–Cr(2)–S(9)	83(2)	
S(7)–Cr(1)–S(11)	90(2)		S(8)–Cr(2)–S(9)	72(2)	
$\overline{S–Cr(1)–S}$	90		$\overline{S–Cr(2)–S}$	89	
		Cr(1)–S(1)–Cr(2) = 95.4(15)			
		Cr(1)–S(2)–Cr(2) = 87.1(16)			

$P(1)S_4$ group		$P(2)S_4$ group		$P(3)S_4$ group	
P(1)–S(7)	2.14(8)	P(2)–S(1)	2.21(3)	P(3)–S(2)	2.13(3)
P(1)–S(8)	2.01(7)	P(2)–S(3)	2.04(9)	P(3)–S(4)	2.15(7)
P(1)–S(9)	2.04(6)	P(2)–S(5)	2.13(6)	P(3)–S(6)	2.10(8)
P(1)–S(11)	2.10(3)	P(2)–S(10)	1.99(2)	P(3)–S(12)	2.06(2)
$\overline{P(1)–S}$	2.07	$\overline{P(2)–S}$	2.09	$\overline{P(3)–S}$	2.11
S(7)–P(1)–S(8)	119(2)	S(1)–P(2)–S(3)	96(2)	S(2)–P(3)–S(4)	96(2)
S(7)–P(1)–S(9)	112.9(17)	S(1)–P(2)–S(5)	91.8(19)	S(2)–P(3)–S(6)	105(2)
S(7)–P(1)–S(11)	115(3)	S(1)–P(2)–S(10)	108.5(12)	S(2)–P(3)–S(12)	116.9(13)
S(8)–P(1)–S(9)	93(3)	S(3)–P(2)–S(5)	115.2(18)	S(4)–P(3)–S(6)	115.6(18)
S(8)–P(1)–S(11)	105(2)	S(3)–P(2)–S(10)	117(2)	S(4)–P(3)–S(12)	114(3)
S(9)–P(1)–S(11)	108(2)	S(5)–P(2)–S(10)	120(3)	S(6)–P(3)–S(12)	109(2)
$\overline{S–P(1)–S}$	109	$\overline{S–P(2)–S}$	108	$\overline{S–P(3)–S}$	109

where $x = -2J/kT$. Using $g = 1.97$, a rather good agreement between the data and the expression of Eq. [1] is obtained with $J/k = -11.07(8)$ K, for $T > 12$ K. This value is quite similar to that reported for $K_6Cr_2P_4S_{16}$, $J/k = -11.52(13)$ K, the structure of which contains isolated Cr_2S_{10} dimers (14). Nevertheless, the fit of the susceptibility of $K_3Cr_2P_3S_{12}$ with Eq. [1] is improved by taking into account secondary magnetic interactions between dimers. Within the molecular field approximation, the susceptibility corrected for the interdimer interactions, $\chi'(T)$, is given by (29)

$$\chi'(T) = \frac{\chi(T)}{1 - (2z'J'/Ng^2\mu_B^2)\chi(T)}, \qquad [2]$$

where $\chi(T)$ is the calculated susceptibility due to isolated dimers, Eq. [1]. J' is the interdimer coupling constant and z' the number of nearest-neighbor binuclear units ($z' = 2$ in the chain ($d_{Cr(1)-Cr(2)} = 6.26(12)$ Å) for $K_3Cr_2P_3S_{12}$). As can be seen in Fig. 4, a good fit of the data with Eq. [2] is obtained above $T > 12$ K; the best fit gives $J/k = -12.9(1)$ K and $z'J'/k = -3.1(1)$ K.

The fitted value of the intradimer magnetic interaction, $J \sim -13$ K, can be compared to predictions based on Goodenough–Kanamori–Anderson rules for exchange and superexchange. For edge-sharing $Cr^{3+}S_6$ octahedra, direct t_{2g}–t_{2g} interactions should have AF character while the superexchange coupling via sulfur should be ferromagnetic for Cr–S–Cr angles close to 90°. Thus, the sign and the

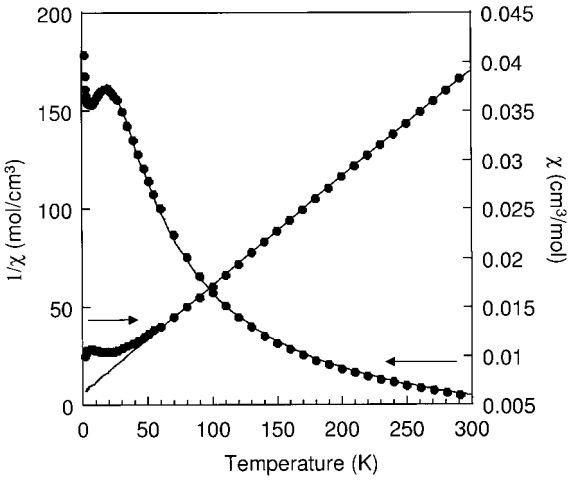

FIG. 4. Temperature dependence of the reciprocal molar magnetic susceptibility ($1/\chi_{mol}$) and the molar magnetic susceptibility (χ_{mol}) per chromium mole corrected for the diamagnetic contribution (solid circles) of $K_3Cr_2P_3S_{12}$. The straight and curve lines correspond to the $1/\chi_{mol}$ and χ_{mol} fit for the temperature ranges 100–300 K and 12–300 K respectively.

magnitude of the net nearest-neighbour Cr–Cr coupling J should depend on the values of the Cr–Cr distance and the Cr–S–Cr angle (30). Based on the work in Ref. (30) and on our crystal data, the intradimer interaction in $K_3Cr_2P_3S_{12}$ is predicted to be about -15 K, and this value is indeed very close to the value extracted from the best fit to the data with Eq. [2].

5. CONCLUDING REMARKS

Our attempts to obtain low-dimensional thiophosphates of chromium and alkali metal in the A/Cr/P/S system was successfully achieved through the synthesis of $Na_3Cr_2P_3S_{12}$ and $K_3Cr_2P_3S_{12}$. After the characterization of these two new phases and the evidencing of their 1D character, experiments have been carried out to test their exfoliation properties. $Na_3Cr_2P_3S_{12}$ crystals swell and dissolve spontaneously in DMF and CH_3CN to give dark green solutions. In contrast, the addition of a 2,2,2-cryptand is requested to dissolve $K_3Cr_2P_3S_{12}$ in DMF, yielding also a dark green solution. It is worth noting that no birefringence is evidenced (even for concentrated solutions) by optical microscopy under polarized light (crossed polarizers), suggesting that the $^1_\infty[Cr_2P_3S_{12}]^{3-}$ chains are not maintained in solution. The chemistry in solution of these phases is currently in progress.

ACKNOWLEDGMENT

E. Kopnin thanks the Conseil Regional des Pays de la Loire for the financial support.

REFERENCES

1. T. J. McCarthy and M. G. Kanatzidis, *Inorg. Chem.* **34,** 1257–1267 (1995).
2. K. Chondroudis and M. G. Kanatzidis, *J. Solid State Chem.* **138,** 321–328 (1998).
3. J. A. Honko and M. G. Kanatzidis, *J. Alloys Compds.* **280,** 71–76 (1998).
4. M. G. Kanatzidis and A. C. Sutorik, *Prog. Inorg. Chem.* **43,** 151–265 (1995).
5. M. G. Kanatzidis, *Curr. Opin. Solid State Mater. Sci.* **2,** 139 (1997).
6. W. Bronger and P. J. Müller, *J. Less-Comm. Met.* **100,** 241–247 (1984).
7. Y. J. Lu and J. A. Ibers, *Comments Inorg. Chem.* **14,** 229–243 (1993).
8. G. Gauthier, S. Jobic, R. Brec, and J. Rouxel, *Inorg. Chem.* **37,** 2332–2333 (1998).
9. G. Gauthier, Thesis, University of Nantes, 1999.
10. G. Gauthier, S. Jobic, V. Danaire, R. Brec, and M. Evain, *Acta Crystallogr. Sect. C* **56,** 117 (2000).
11. E. Kopnin, S. Coste, S. Jobic, M. Evain, and R. Brec, *Mater. Res. Bull.* **35,** 1401–1410 (2000).
12. S. Coste, E. Kopnin, M. Evain, S. Jobic, R. Brec, K. Chondroudis, and M. Kanatzidis, submitted for publication.
13. W. Tremel, H. Kleinke, V. Derstroff, and C. Reisner, *J. Alloys Compds.* **219,** 73–82 (1995).
14. V. Derstroff, V. Ksenofontov, P. Gütlich, and W. Tremel, *Chem. Commun.* 187–188 (1998).
15. J. Sayettat, L. Bull, J.-C. Gabriel, S. Jobic, F. Camerel, A.-M. Marie, M. Fourmigué, P. Batail, R. Brec, and R.-L. Inglebert, *Angew. Chem. Int. Ed.* **37,** 1711–1714 (1998).
16. J. Sayettat, L. Bull, S. Jobic, J. C. Gabriel, M. Fourmigué, P. Batail, R. Brec, R.-L. Inglebert, and C. Sourisseau, *J. Mater. Chem.* **9,** 143–153 (1999).
17. P. Davidson, J.C. Gabriel, A-M. Levelut, and P. Batail, *Europhys. Lett.* **21,** 317–322 (1993).
18. P. Davidson, J. C. Gabriel, A.-M. Levelut, and P. Batail, *Adv. Mater.* **5,** 665–668 (1993).
19. J. M. Tarascon, F. G. DiSalvo, C. H. Chen, P. J. Caroll, M. Walsh, and L. Rupp, *J. Solid State Chem.* **58,** 290–300 (1985).
20. J. H. Liao and M. G. Kanatzidis, *Inorg. Chem.* **31,** 431–439 (1992).
21. Stoe IPDS software, STOE & Cie GmbH, Darmstadt, Germany (1996).
22. G. M. Sheldrick, SHELXTL version 5, Siemens Analytical X-Ray Instruments, Madison, WI.
23. V. Petricek and M. Dusek, JANA2000, Institute of Physics, Academy of Sciences of the Czech Republic, Prague, Czech Republic (2000). M. Dusek, V. Petricek, M. Wunschel, R. E Dinnebier, and S. van Smaalen, *J. Appl. Cryst.*, submitted.
24. A. Le Bail, H. Duroy, and J. L. Fourquet, *Mater. Res. Bull.* **23,** 447–452 (1988).
25. H. M. Rietveld, *J. Appl. Cryst.* **2,** 65–71 (1969).
26. R. D. Shannon, "Structure and Bonding in Crystals." Academic Press, San Diego, 1981.
27. "Landolt–Börstein Tables," Vol. I, Part 1, pp. 395–398. Springer-Verlag, Berlin, 1950.
28. R. Carlin, "Magneto-chemistry," Chap. 5. Springer-Verlag, Berlin, 1986.
29. C. J. O'Connor, *Prog. Inorg. Chem.* **29,** 203 (1982).
30. P. Colombet and M. Danot, *Solid State Commun.* **45,** 311–315 (1983), and references therein.
31. J. F. Berar and P. Lelann, *J. Appl. Cryst.* **24,** 1–5 (1991).
32. L. W. Finger, D. E. Cox, and A. P. Jephcoat, *J. Appl. Cryst.* **27,** 892–900 (1994).
33. W. A. Dollase, *J. Appl. Cryst.* **19,** 262–272 (1986).
34. A. March, *Z. Kristallogr.* **81,** 285–297 (1932).